Journal of Applied Physics

Effect of amorphization-mediated plasticity on the hydrogen-void interaction in ideal lattices under hydrostatic tension

Cite as: J. Appl. Phys. **123**, 245101 (2018); https://doi.org/10.1063/1.5029953
Submitted: 17 March 2018 . Accepted: 09 June 2018 . Published Online: 22 June 2018

Kai Zhao, Jianying He, Inga Gudem Ringdalen, and Zhiliang Zhang

Effect of amorphization-mediated plasticity on the hydrogen-void interaction in ideal lattices under hydrostatic tension

Kai Zhao,[1] Jianying He,[1] Inga Gudem Ringdalen,[2] and Zhiliang Zhang[1,a)]
[1]*NTNU Nanomechanical Lab, Department of Structural Engineering, Norwegian University of Science and Technology (NTNU), Trondheim 7491, Norway*
[2]*SINTEF Materials and Chemistry, Trondheim 7491, Norway*

(Received 17 March 2018; accepted 9 June 2018; published online 22 June 2018)

A thermodynamic model is derived to study the void nucleation in ideal lattices under hydrostatic tension loading and predicts that the plasticity has to be initiated before homogeneous nucleation of voids. Molecular dynamics simulations are performed to evaluate the mechanical behavior of Ni specimens with and without hydrogen charged. The results show that in both cases dislocations are generated before the nucleation of voids, and the insertion of hydrogen atoms does not alter the void nucleation significantly. The fact that the mechanical property is not sensitive on hydrogen is attributed to the formation of an amorphous shell around the voids. *Published by AIP Publishing.*
https://doi.org/10.1063/1.5029953

I. INTRODUCTION

Ductile fracture in metals commonly occurs by the nucleation, growth, and coalescence of voids. Capturing the complete evolution path of voids across scales is thus essential to understand the fundamental physics beneath the critical consequences, such as spallation,[1] softening due to void growth,[2] plastic localization,[3] cavitation instabilities,[4,5] as well as the intriguing hydrogen-induced ductile to brittle transition.[6] The commonly cited continuum mechanics models, such as the Rice-Tracy,[7] Gurson-Tvergaard-Needleman,[8,9] and Rousselier model,[10] can properly describe the growth and coalescence of pre-existing voids. These models, however, fail to predict ductile fracture at atomistic scale.[11,12] Thus, understanding the intrinsic mechanisms underlying the evolution of void dynamics requires the atomistic knowledge of localized deformation.[1,13] Verified by both atomistic simulations[12,14–17] and experiments,[17,18] it is well established that the nanoscale void growth is driven by dislocation-mediated plastic deformation.[1,17,19,20] Compared with the growth of an existing void, little is known about the nucleation of voids itself. In polycrystalline materials, void nucleation occurs heterogeneously by cracking at grain boundary,[21,22] de-bonding at particle/inclusion-matrix interface,[23] or breaking of particles.[24] However, the homogeneous nucleation without the presence of preferred nucleation sites in ideal lattice is not well understood. Taking the well-defined hydrostatic loading as an example, whether and how the dislocation plasticity interacts with the atomistic void nucleation process remains an open question. Meanwhile, given the fact that hydrogen has been envisioned to stabilize and promote the agglomeration of vacancies,[25,26] thus leading to the lowering of ductility through the growth and coalescence of nanovoids,[6] it is necessary to understand the effect of hydrogen on the homogeneous void nucleation process, especially the interaction between hydrogen solutes and the plastic flow around a nanovoid quantitatively.

In this manuscript, following the merit of the previous studies,[27–30] we will start by describing the free energy model of void nucleation accompanied with plastic deformation based on the study of cavitation process in amorphous solids.[28] We then perform MD simulations of both pure Ni and Ni-H system to calibrate and verify the free energy model.

II. METHODOLOGY

It is reasonable to regard liquid as an extreme case of plastically deformed solids[31] and draw a parallel between cavitation in liquids and void nucleation in solids. Therefore, quoting the study of metallic glass,[28] the free energy change upon creation of an embryo of a void is given by

$$\Delta G = E_e - E_s - W_p, \tag{1}$$

where ΔG is the free energy change due to void nucleation, which can be decomposed into contributions from the bulk elastic response $E_e = \frac{4}{3}\pi r^3 K\varepsilon$, the surface tension $E_s = 4\pi r^2\gamma$, and the plastic dissipation W_p, where K is the bulk modulus, ε is the volumetric strain at the remote boundary, r is the void radius, and γ is the surface energy. To a first approximation, we assume that the plastic dissipation scales only with the void volume and define ε_c via the equivalency $W_p \equiv K\varepsilon_c V_c$, where $V_c = \frac{4}{3}\pi r^3$ is the volume of the cavity. The surface energy is known to be curvature dependent at small radii, and a form for this dependence was proposed by Tolman,[32,33] in which $\gamma = \gamma_\infty/(1 + 2\delta/r)$, where γ_∞ is the surface energy of the flat surface and δ is a parameter known as the Tolman length. If the void is spherical and grows monotonically, we can solve the critical void radius at which the void becomes unstable by differentiating Eq. (1) as

$$dG/dr = 4\pi r^2\left[K(\varepsilon - \varepsilon_c) - 3\frac{\gamma_\infty}{r + 2\delta} + r\frac{\gamma_\infty}{(r + 2\delta)^2}\right]. \tag{2}$$

a)Author to whom correspondence should be addressed: zhiliang.zhang@ntnu.no

Let Eq. (2) equals to zero, we can obtain the critical void radius

$$r_c = r^*\left(\frac{1}{2}+\frac{1}{2}\sqrt{1+\frac{4\delta}{r^*}}-\frac{2\delta}{r^*}\right), \tag{3}$$

where $r^* = 2\gamma_\infty/K(\varepsilon-\varepsilon_c)$ represents the critical radius for the case where the surface energy is independent of curvature ($\delta = 0$). By integrating Eq. (2), the free energy barrier for cavitation is

$$\Delta G_c = \frac{4}{3}\pi r_c^3 K(\varepsilon-\varepsilon_c) - 4\pi\gamma r_c^2. \tag{4}$$

As shown in Fig. S1 (Supplementary Material), by numerically solving Eq. (4), we can obtain the direct insights about the Gibbs free energy as a function of hydrostatic tension under static relaxation.

According to the classical nucleation theory,[27] the nucleation rate at any moment can be written as

$$\nu = \nu_0 \exp\left(\frac{\Delta G}{k_B T}\right), \tag{5}$$

where ν_0 is the attempt frequency, and the nucleation rate refers to per atom scenario. For the homogeneous cavitation under constant-rate tension, the probability of solid phase containing cavities should be constant,[27,31] i.e.,

$$p = 1 - \exp\left\{-\frac{\int_0^{\varepsilon_f}\nu \mathrm{d}\varepsilon}{\zeta}\right\}. \tag{6}$$

Here, Cai *et al.*[27] have demonstrated the equivalence between temporal and spatial scale inherent in the nucleation events in liquid Cu by proposing a size-rate parameter $\zeta = \dot{\varepsilon}/N$. If we describe the hydrostatic stress with a naïve linear elasticity, Eq. (6) can be analytically reformulated as

$$p(\varepsilon) = 1 - \exp\left\{-\frac{3k_BT\nu_0}{4\pi r^3 K\zeta}\left\{\exp\left[-\frac{4\pi r^3}{3k_BT}\left(\frac{3\gamma}{r}-K(\varepsilon-\varepsilon_c)\right)\right] - \exp\left[-\frac{4\pi r^2}{k_BT}\gamma\right]\right\}\right\}. \tag{7}$$

It should be noted that the critical void radius derived in Eq. (3) could not be applied here because the equilibrium relaxation is not satisfied under dynamic loading. In order to verify the proposed model above and investigate the H effect on the cavitation in metals, we carry out MD simulations using LAMMPS code.[34] The embedded atom method potential proposed by Angelo *et al.*[35] is used to describe the pairwise interactions between Ni and H atoms. The grand canonical Monte Carlo[36] relaxation is employed to introduce the H atoms into the fcc lattice by establishing the optimum lattice configurations in thermal equilibrium with an imposed hydrogen reservoir. Initially, the system is relaxed under the NPT ensemble with constant temperature (300 K) and pressure (0 bar). Then, the constant stain rate loading is applied on the specimen under the canonical (NVT) ensemble with the temperature fixed at 300 K. For the simulation with a given specimen size and strain rate, we carry out 60–100 independent runs in order to provide sufficient sampling depending on the computational costs.

III. RESULTS

Under hydrostatic tension, the typical process of the stress evolution for specimens both without and with hydrogen charged are presented in Fig. 1, along with the inserted snapshots of void nucleation and growth at representative moments. Statistical analysis shows that the insertion of hydrogen atoms seems to not affect the fracture behavior significantly. The initial negative value of the hydrostatic stress in NiH system indicates that the hydrogen gives rise to the existence of internal pressure. From another standpoint, it also means that an external pressure is required to charge the hydrogen atoms into the specimen. For the pure Ni specimen, it is clearly observed that the dislocation loop is nucleated before the sudden drop of the hydrostatic stress. The snapshots of NiH system indicate that the dislocation activities are closely coupled with the formation of a void. Besides, the formation of an amorphous shell around the void is also observed in Fig. S3 (Supplementary Material), which originates from the local rearrangement of atoms and represents another kind of plastic dissipation.[28] Thus, the MD results confirm the predictions of Fig. S1 (Supplementary Material), i.e., plasticity must be initiated before the nucleation of voids irrespective of the insertion of hydrogen atoms.

In order to explore the effect of the interplay between size and strain rate on the fracture behavior, we calculate the hydrostatic stress-strain curves of specimens with three different sizes under five different strain rates (10^6, 10^7, 2×10^7, 5×10^7, and 10^8/s). The statistical distribution of the critical failure strain ε_f is shown as a function of strain rate in Fig. 2, which contains more than 1000 independent

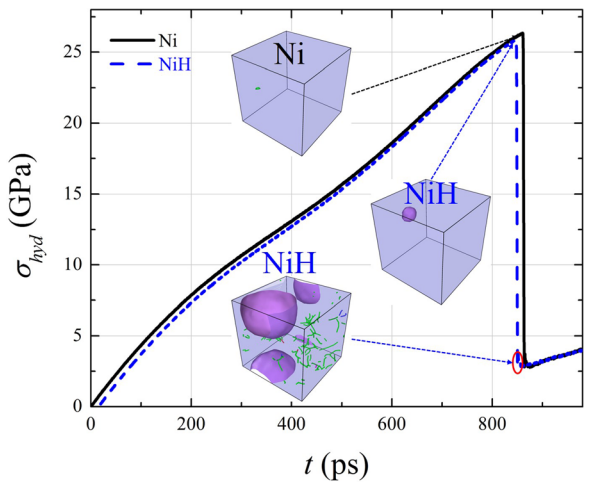

FIG. 1. The hydrostatic stress vs. time for both Ni and NiH systems under constant strain rate of 10^8/s with the same amount of Ni atoms ($20\times20\times20$ a_0^3). The inserted snapshot of Ni specimen illustrates a dislocation loop is nucleating, but not necessarily the first nucleation event. The two snapshots of NiH specimen represent the void nucleation and subsequent growth associated with dislocation multiplication, respectively. The green lines represent dislocation network, while the purple bulb is the nanovoid.

stress-strain tests, thus guarantees that the effect of thermal fluctuation can be well considered. It is found that the statistical average of ε_f increases monotonically with the strain rate, while decreases with the specimen size. However, the insertion of hydrogen atoms seems not significantly alter the statistical distribution of ε_f. That is to say, hydrogen almost exerts no influence on collective behavior of dislocation generation and lattice decohesion. Previous studies of Ni single crystal with hydrogen pre-charged[37] also lead to the similar conclusions. While for the single crystal specimens with hydrogen dynamically charged[37] or the bicrystal specimens,[38] hydrogen will result in severe decrease in the failure strain due to the heterogeneous nucleation of nanovoids at lattice defects. It should be noticed that Jiang and Carter[39] have found that the surface energy deceases with the increase in the hydrogen coverage by density functional theory calculations, where the hydrogen concentration is astronomically large. However, when the DFT calculations are performed

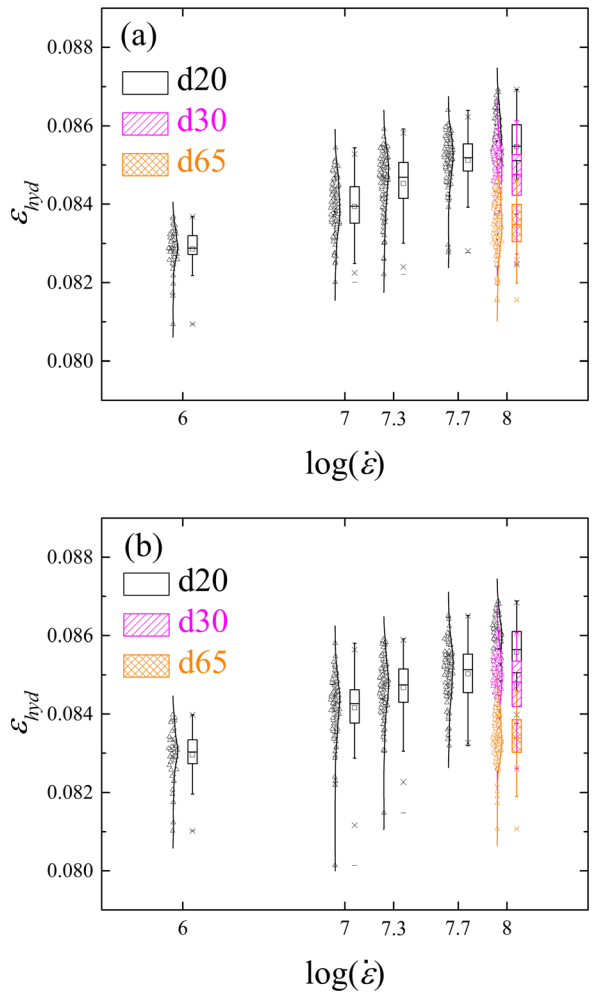

FIG. 2. The critical hydrostatic failure strain as a function of the strain rate. Each open triangle symbol represents a single hydrostatic tension test, while this figure contains more than 1000 tests in total. (a) for pure Ni single crystal and (b) for Ni-H system. The black blank box (d20) represents the system with 32 000 Ni atoms ($20 \times 20 \times 20$ a_0^3), magenta diagonal stripe pattern (d30) with 1 08 000 Ni atoms ($30 \times 30 \times 30$ a_0^3), and orange textile pattern (d65) with 10 98 500 Ni atoms ($65 \times 65 \times 65$ a_0^3) with a_0 being the lattice constant. The dynamic loading tests are performed for d20 specimens under five different strain rates, while the d30 and d65 specimens are only loaded under 10^8/s due to the limitation of computational resources.

under practical hydrogen concentration, the difference of surface energy per atom could be ignored. Thus, the inserted hydrogen atoms could only affect the plastic dissipation process, where the strong interaction between dislocation-mediated plasticity and hydrogen atmosphere has been validated.[40] Thus, the insensitivity of hydrogen on the void nucleation shown in Fig. 2 indicates that the hydrogen-dislocation interaction may be suppressed by the formation of the amorphous shell. In Fig. 3(a), the median values of ε_f in different subgroups in Fig. 2 are plot as a function of the parameter $1/\zeta$. It is found that the effect of specimen size and loading rate on the fracture behavior can be universally described by introducing the scaling factor ζ. The comparison between Ni and Ni-H systems indicates that the ε_f is almost not influenced by the insertion of hydrogen atoms. As the value of $N/\dot{\varepsilon}$ approaches positive infinite, which represents the normal laboratory condition, the failure strain decays to finite value slowly. Implicitly, Eq. (7) indicates that the physical quantities like void radius, Tolman length, and characteristic plastic strain may be a function of ζ, while other quantities like bulk modulus and remote surface energy would not change with specimen size and strain rate. It has to be mentioned that this universal law only accounts for the dislocation mediated plastic dissipation as the only internal process during ductile cavitation, while in realistic experiments/simulations, other types of dissipation processes, such as precipitation hardening and grain boundary migration, cannot be ignored and will definitely lead to the difference with the predictions of this scaling law. In Fig. 3(b), temporarily forget the plasticity, a typical example of the cavitation probability [exactly Eq. (7)] is shown with respect to the applied volumetric strain, where a sharp transition from 0 to 1 is identified as the critical failure strain ε_f. In Figs. 3(c) and 3(d), we plot the contours of the critical failure strain ε_f as a function of the Tolman length δ and nucleus radius r for $\varepsilon_c = 0$ and 0.08, respectively. It is found that when the plastic effect is ignored, the maximum failure strain for void nucleation is $\sim$0.123 and the most probable failure strain is localized in the range of [0.001, 0.01625]. In Fig. 3(d), by assigning an attempt $\varepsilon_c = 0.08$, the most probable failure strain will be elevated to the range of [0.07675, 0.1020]. Thus, the introduction of initial plasticity can effectively enhance the ductility of metals. Provided the characteristic ε_c and ε_f can be obtained from experiments/simulations, the possible range of the initial void radius can be directly derived from Fig. 3(d) with the Tolman length δ and ζ known. Further calculations indicate that the slight variation of ζ does not alter the distribution of critical failure strain, thus the dependency shown in Fig. 3(a) can only originate from the change of void size and/or the Tolman length.

As the cavitation process under dynamic loading has been clarified, we study the natural nucleation of voids under quasi-static loading now. Considering the scenario that the system is loaded to a given state, the atomic configuration of which will be recorded and relaxed under NVT ensemble. In order to eliminate the effect of thermal fluctuation, for each instinct configuration, 100 independent runs are carried out. The cavitation event is identified by monitoring the sudden decrease in the potential energy, with details shown in the

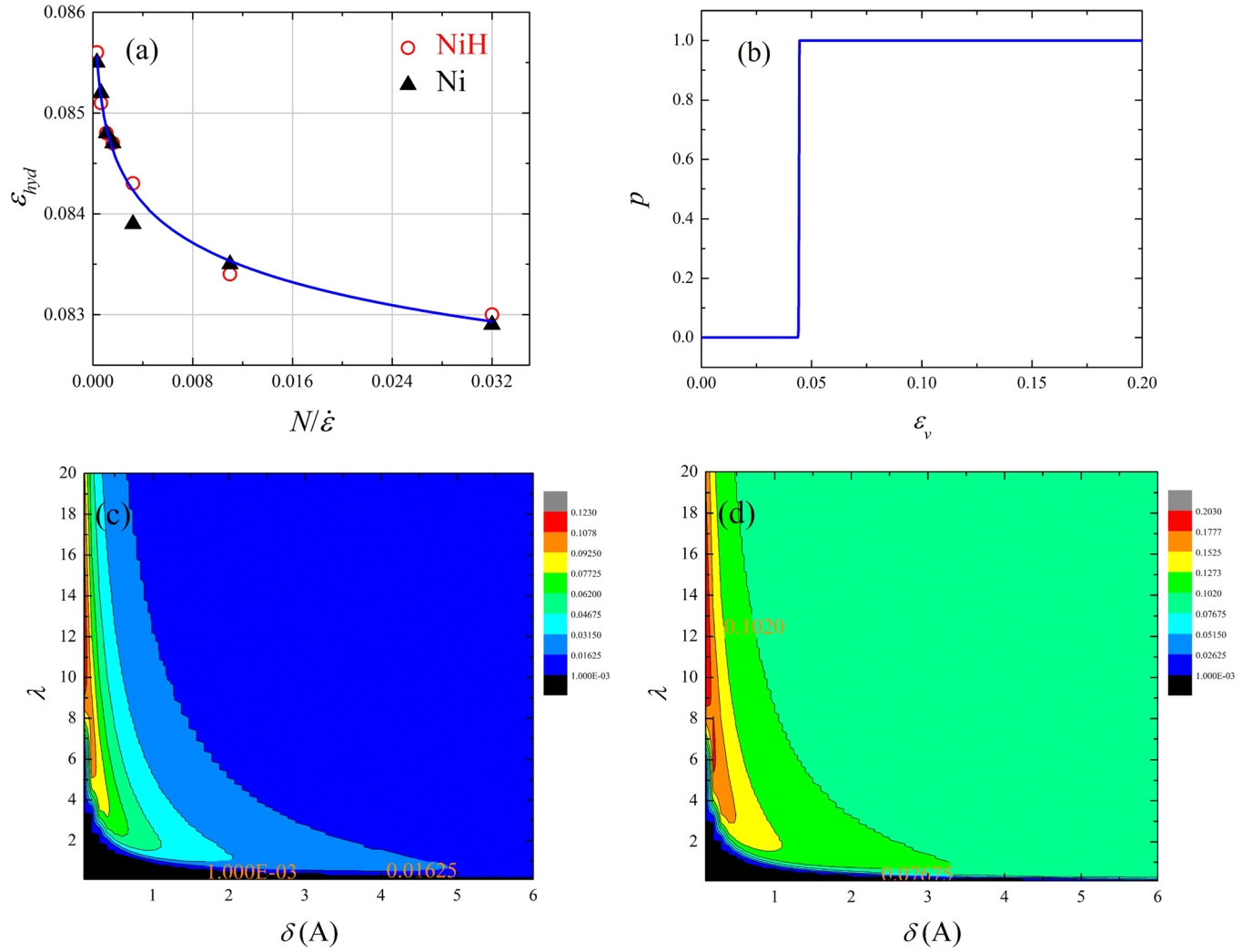

FIG. 3. (a) The critical failure strain as a function of the parameter $\zeta = N/\dot{\varepsilon}$ for both Ni and Ni-H systems. The blue curve is fitted to the function $y = A/x^B$ with parameters $A = 0.08102$ and $B = 0.00677$ and is shown as a guide to the eye. (b) A typical plot of the cavitation probability as a function of the volumetric strain with $\delta = 0.5$ Å and $\lambda = 8$. (c) The contour map of the critical failure strain under linear elasticity (i.e., $\varepsilon_c = 0$). (d) The contour map of the critical failure strain with an attempt $\varepsilon_c = 0.08$. Here, we define the dimensionless parameter $\lambda = r/\delta$, i.e., the void radius normalized by the Tolman length.

supplementary material. If the cavitation process is a homogeneous Poisson process under a given strain, the fraction of the cavitated samples described by Eq. (6) decays into $f_\varepsilon^T(t) = 1 - e^{-NR_\varepsilon^T t_f}$, with treating the nucleation rate $\upsilon = R_\varepsilon^T$ as a single time constant, i.e., the rate of cavitation per atom per unit time, and $t_f = \varepsilon_f/\dot{\varepsilon}$ as the fracture time. Thus, with a given $N/\dot{\varepsilon}$, the nucleation probability is implicitly a function of ε_c, δ, and ε_f, if we assume that the surface energy and bulk modulus are not affected due to the charging of hydrogen. As shown in Fig. 4(a), a plot of $\ln\left(1 - f_\varepsilon^T(t)\right)$ as a function of time t does behave in a linear fashion over the entire time window for both Ni and Ni-H systems. It is of no interest to compare the absolute value of the fitted slope, because the thermal fluctuation (k_BT) is on the same order of the activation energy. The direct information derived from Fig. 4(a) is that the insertion of hydrogen atoms does not alter the Poisson feature of the nucleation process. The results thus demonstrate that H atoms seem to be evenly smeared in the ideal lattice, rather than to be introduced as heterogeneous sites. Dongare *et al.*[41] have found that the void growth in Cu occurs by the formation of a shell of disordered atoms, which results in the amorphous-like response in the local region around the voids. Experimentally, the deformation induced crystalline to amorphous transition in single crystal Si has been evidenced by the *in situ* TEM observations.[42] The observation of large amount of disordered atoms in this study (see the supplementary material) thus guarantees the application of Poisson process. In a previous experimental study, Liu *et al.*[43] have found that the tensile response of Zr-based bulk amorphous alloys is not sensitive to the environmental hydrogen at room temperature. In the study of the mechanical properties of amorphous $Fe_{40}Ni_{38}Mo_4B_{18}$, Lin and Perng[44] found that the effect of hydrogen on the tensile strength of reduced-section specimens under various strain rates is negligible, while the fracture toughness of double-edge-notched specimens is significantly reduced due to the presence of hydrogen at lower strain rates. These results may indicate that the hydrogen embrittlement is attributed to the heterogeneous nucleation of localized plastic deformation,[45] which is absent in present high strain rate MD simulations. It should be mentioned that plastic flow still occurs during the deformation of amorphous solids.[28] Thus, our understanding

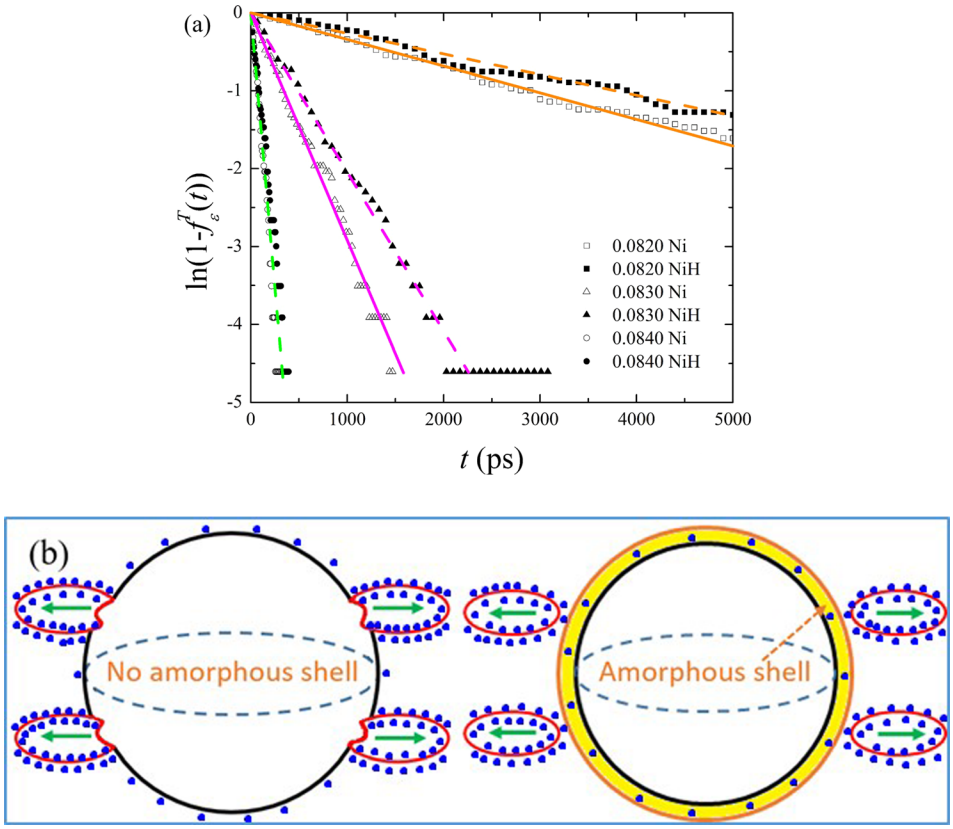

FIG. 4. (a) The value of $\ln\left(1-f_\varepsilon^T(t)\right)$ as a function of t, where f_ε^T is the fraction of samples that have been cavitated. The open and solid symbols represent the Ni and NiH systems at corresponding hydrostatic strain (extracted from the stress-strain curves shown in Fig. 1), respectively. The dashed and solid lines are used to illustrate the linear feature with fixed intercept at 0. (b) Left panel: The void growth by attached shear loops. Right panel: The amorphous shell suppresses the dislocation-based void activities, with the blue points representing H atoms.

of hydrogen-plasticity interaction should be widened that there may exist a competition between the dislocation- and amorphization-mediated plasticity processes. Although we cannot decouple the effect of plasticity and surface tension in the present data processing procedure, the hydrogen does not exert significant effect on the resultant coupled process, thereby cannot precisely modify these two dissipation behaviors independently. That is to say, the interactions between hydrogen and dislocations are not directly observed during the homogeneous nucleation of voids. As shown in Fig. 4(b), while it is already confirmed that the void grow is promoted by the emission and multiplication of dislocations attached on the void surface (in the left panel), the presence of hydrogen will definitely accelerate the void dynamics if the hydrogen enhanced localized plasticity mechanism is present, which is realized either by the enhanced dislocation mobility or nucleation (in the right panel). Furthermore, the fitted slope of MD results also indicates that the absolute value of ΔG_c deceases with the applied strain as predicted by Eq. (4) (see Fig. S1). Thus, with the critical failure strain known from simulations or experiments, the physical quantities ε_c and δ can be obtained by fitting these ΔG_c data to Eq. (4). Given by the slight difference of ε_f between Ni and NiH systems shown in Fig. 1, no significant effect of H on the plasticity and surface tension can be expected.

IV. CONCLUSIONS

In summary, for the first time, it is confirmed mathematically and atomically that the initiation of plasticity is a sine qua non of homogeneous void nucleation in crystalline materials, while the necessary plastic activity involves the contributions from the formation of an amorphous shell as well as the nucleation and movement of dislocations. When the statistical error is considered, the hydrogen-induced decrease in the critical failure stain observed in the previous studies may need to be revisited. MD results show that there exists no significant variation of the critical failure strain due to the insertion of H atoms. The insensitivity of hydrogen charging could originate from the formation of an amorphous shell, which masks the effect of hydrogen on the plasticity-mediated process of void nucleation. These results may urge a reconsideration of the "shielding" effect of the amorphous shell on the interactions between hydrogen and nanovoid. Together with the previous experimental studies, this paper further points out that the addition of amorphous phase in metallic materials may improve the resistance of hydrogen embrittlement. The plot of the failure strain as a function of the size-rate parameter ζ can be employed to bridge the gap between the information obtained from the atomistic simulations and continuum scale experiments. Informed by MD simulations, the thermodynamic model predicts that the insertion of hydrogen atoms does not exert considerable influence on the homogeneous nucleation of nanovoids. It thus suggests that the operation of the nanovoid coalescence mechanism[6] of hydrogen embrittlement depends on the hydrogen enhanced heterogeneous nucleation of voids on microstructural defects.

SUPPLEMENTARY MATERIAL

See supplementary material for the details of the free energy model, MD settings, and the formation of amorphous shells.

ACKNOWLEDGMENTS

This work was supported by the Research Council of Norway under Grant No. 234130/E30. All simulations were carried out on the NOTUR high performance computer clusters under Grant Nos. NN9110K and NN9391K.

[1]J. Marian, J. Knap, and M. Ortiz, Phys. Rev. Lett. **93**, 165503 (2004).
[2]N. A. Fleck, J. W. Hutchinson, and V. Tvergaard, J. Mech. Phys. Solids **37**, 515–540 (1989).
[3]V. Tvergaard, J. Mech. Phys. Solids **35**, 43–60 (1987).
[4]V. Tvergaard, J. Mech. Phys. Solids **44**, 1237–1253 (1996).
[5]Y. Huang, J. W. Hutchinson, and V. Tvergaard, J. Mech. Phys. Solids **39**, 223–241 (1991).
[6]T. Neeraj, R. Srinivasan, and J. Li, Acta Mater. **60**, 5160–5171 (2012).
[7]J. R. Rice and D. M. Tracey, J. Mech. Phys. Solids **17**, 201–217 (1969).
[8]A. Needleman, V. Tvergaard, and J. W. Hutchinson, "Void growth in plastic solids," in *Topics in Fracture and Fatigue*, edited by A. S. Argon (Springer, New York, NY, 1992), pp. 145-178.
[9]A. L. Gurson, J. Eng. Mater. Technol. **99**, 2 (1977).
[10]G. Rousselier, Nucl. Eng. Des. **105**, 97–111 (1987).
[11]C. W. Mi, D. A. Buttry, P. Sharma, and D. A. Kouris, J. Mech. Phys. Solids **59**, 1858–1871 (2011).
[12]S. Traiviratana, E. M. Bringa, D. J. Benson, and M. A. Meyers, Acta Mater. **56**, 3874–3886 (2008).
[13]J. Marian, J. Knap, and M. Ortiz, Acta Mater. **53**, 2893–2900 (2005).
[14]K. Zhao, I. G. Ringdalen, J. Y. Wu, J. Y. He, and Z. L. Zhang, Comput. Mater. Sci. **125**, 36–50 (2016).
[15]Y. Tang, E. M. Bringa, and M. A. Meyers, Acta Mater. **60**, 4856–4865 (2012).
[16]E. M. Bringa, S. Traiviratana, and M. A. Meyers, Acta Mater. **58**, 4458–4477 (2010).
[17]V. A. Lubarda, M. S. Schneider, D. H. Kalantar, B. A. Remington, and M. A. Meyers, Acta Mater. **52**, 1397–1408 (2004).
[18]T. P. Remington, B. A. Remington, E. N. Hahn, and M. A. Meyersa, Mater. Sci. Eng. A **688**, 429–458 (2017).
[19]E. T. Seppälä, J. Belak, and R. E. Rudd, Phys. Rev. Lett. **93**, 245503 (2004).
[20]E. T. Seppala, J. Belak, and R. E. Rudd, Phys. Rev. B **69**, 134101 (2004).
[21]D. Farkas, S. Van Petegem, P. M. Derlet, and H. Van Swygenhoven, Acta Mater. **53**, 3115–3123 (2005).
[22]P. Shewmon and P. Anderson, Acta Mater. **46**, 4861–4872 (1998).
[23]A. Needleman, J. Appl. Mech. **54**, 525–531 (1987).
[24]H. G. F. Wilsdorf, Mater. Sci. Eng. **59**, 1–39 (1983).
[25]M. Nagumo, Mater. Sci. Technol. **20**, 940–950 (2004).
[26]M. Nagumo, ISIJ Int. **41**, 590–598 (2001).
[27]Y. Cai, J. Y. Huang, H. A. Wu, M. H. Zhu, W. A. Goddard, and S. N. Luo, J. Phys. Chem. Lett. **7**, 806–810 (2016).
[28]P. Guan, S. Lu, M. J. B. Spector, P. K. Valavala, and M. L. Falk, Phys. Rev. Lett. **110**, 185502 (2013).
[29]D. W. Nicholson, Acta Mech. **34**, 263–266 (1979).
[30]V. I. Levitas and N. S. Altukhova, Acta Mater. **59**, 7051–7059 (2011).
[31]Y. Cai, H. A. Wu, and S. N. Luo, J. Chem. Phys. **140**, 214317 (2014).
[32]R. C. Tolman, J. Chem. Phys. **17**, 333–337 (1949).
[33]Q. An, G. Garrett, K. Samwer, Y. Liu, S. V. Zybin, S.-N. Luo, M. D. Demetriou, W. L. Johnson, and W. A. Goddard, J. Phys. Chem. Lett. **2**, 1320–1323 (2011).
[34]S. Plimpton, J. Comput. Phys. **117**, 1–19 (1995).
[35]J. E. Angelo, N. R. Moody, and M. I. Baskes, Modell. Simul. Mater. Sci. Eng. **3**, 289 (1995).
[36]D. Frenkel and B. Smit, *Understanding Molecular Simulation*, 2nd ed. (Academic Press, San Diego, 2002), pp. 111-137.
[37]M. Q. Chandler, M. F. Horstemeyer, M. I. Baskes, P. M. Gullett, G. J. Wagner, and B. Jelinek, Acta Mater. **56**, 95–104 (2008).
[38]M. Q. Chandler, M. F. Horstemeyer, M. I. Baskes, G. J. Wagner, P. M. Gullett, and B. Jelinek, Acta Mater. **56**, 619–631 (2008).
[39]D. E. Jiang and E. A. Carter, Acta Mater. **52**, 4801–4807 (2004).
[40]H. K. Birnbaum and P. Sofronis, Mater. Sci. Eng. A **176**, 191–202 (1994).
[41]A. M. Dongare, A. M. Rajendran, B. LaMattina, M. A. Zikry, and D. W. Brenner, Phys. Rev. B **80**, 104108 (2009).
[42]Y. C. Wang, W. Zhang, L. Y. Wang, Z. Zhuang, E. Ma, J. Li, and Z. W. Shan, NPG Asia Mater. **8**, e291 (2016).
[43]C. T. Liu, L. Heatherly, D. S. Easton, C. A. Carmichael, J. H. Schneibel, C. H. Chen, J. L. Wright, M. H. Yoo, J. A. Horton, and A. Inoue, Metall. Mater. Trans. A **29**, 1811–1820 (1998).
[44]J. J. Lin and T. P. Perng, J. Mater. Sci. Lett. **10**, 1443–1445 (1991).
[45]N. Eliaz and D. Eliezer, Adv. Perform. Mater. **6**, 5–31 (1999).